IEEE Access
Multidisciplinary | Rapid Review | Open Access Journal

Received 9 September 2022, accepted 10 October 2022, date of publication 19 October 2022, date of current version 27 October 2022.

Digital Object Identifier 10.1109/ACCESS.2022.3215551

RESEARCH ARTICLE

Koopman Kalman Particle Filter for Dynamic State Estimation of Distribution System

KAI WANG, MIN LIU, WANG HE, CHAOWEN ZUO, AND FANYUN WANG
School of Electrical Engineering, Guizhou University, Guiyang, Guizhou 550025, China

Corresponding author: Min Liu (ee.mliu@gzu.edu.cn)

This work was supported in part by the National Natural Science Foundation of China under Grant 51967004.

ABSTRACT Dynamic state estimation (DSE) plays an important role in the real-time control and monitoring of distribution systems, which are high-dimensional space–time systems. The degree of nonlinearity of distribution system increases drastically with the availability of sustainable energy and the diversification of load types, thereby reducing the accuracy of the standard linear model. Under the existing schemes, the measurement noise may not follow a Gaussian distribution. Therefore, a Koopman operator-based Kalman particle filter (KKPF) is proposed herein for estimating the dynamic states of a distribution system. The KKPF performs data-driven dynamic state estimation based on the Koopman operator theory, which does not rely on the distribution system model and can be applied to high-dimensional systems. Furthermore, this method can be applied to dynamic systems and noise with both Gaussian and non-Gaussian distributions. The KKPF method provides accurate estimation results when only a small number of measurements are available. IEEE 141 system and an improved 141 system were used to test the performance of the proposed KKPF compared to the EKF, CKF, and PF. The test revealed that the proposed KKPF can obtain accurate results under high-dimensional and non-Gaussian noise environments.

INDEX TERMS Distribution system, dynamic state estimation (DSE), Koopman operator, Koopman mode decomposition, Kalman filter, particle filter.

I. INTRODUCTION

Distribution systems never operate under steady-state conditions because the demand and generation vary stochastically. This situation is exacerbated by the large-scale integration of distributed energy resources, complex loads, and new demand-response technologies, such as electric vehicles and internet-of-things devices on the demand side. The DSE can accurately capture the dynamics of system states and plays an important role in the control and protection of distribution systems [1], [2], [3], [4], particularly with the increasing complexity caused by the uncertainties associated with new technologies [5].

There can be hundreds or tens of thousands of nodes in a distribution system. With an increase in renewable energy sources and load types, the degree of nonlinearity of the distribution system increases significantly [6], decreasing the accuracy of the standard linear model [7], [8]. The power system model is typically not accurately known because of the complexity and dynamism of the power systems. The model and noise statistical uncertainties were both included in these uncertainties. In addition, measurements cannot reflect the dynamics of a power system subjected to SCADA's slow scanning rate. Therefore, because of the complexity and dynamism of power systems, it is challenging to develop an accurate power system model and obtain noise statistics. As the size of power systems increases significantly and renewable energy sources quickly penetrate, the complexity and dynamism of power systems continues to increase [9]. In [10], the states were predicted using the M-estimation approach. The linear exponential smoothing method was used to predict the states [11], [12]. In [13], artificial neural network is used to anticipate the bus load and state, while considering the power system dynamics associated with the change in bus load. However, it is difficult to create a precise state prediction model owing to the complexity and dynamics of

The associate editor coordinating the review of this manuscript and approving it for publication was Min Wang.

the power systems. This results in an increase in the demand for more trustworthy DSE techniques.

Kalman filters (KF), which provide both current and expected states concurrently, have been extensively explored for their ability to forecast the states in the upcoming instant, which is useful for power system security monitoring and control [10], [11], [12], [13], [14]. The challenge with forecasting-aided DSE techniques is modeling the state prediction model and performing DSE with a constrained set of observations [15], [16], [17], [18]. The extended Kalman filter (EKF) can be used to address the forecasting-aided DSE problem. The EKF uses a first-order Taylor series expansion, which may yield unreliable results in the case of a strongly nonlinear system. An unscented Kalman filter (UKF) [19], [20], which approximates the mean and covariance via an unscented transformation, is recommended as a solution to this problem. The cubature Kalman filter (CKF) is a particular instance of UKF. Although it improves the numerical stability and scalability issues of the UKF, it still has drawbacks for high-dimensional systems because of the ''nonlocal sampling problem'' [21]. The ensemble Kalman filter (EnKF) was created in [18] at the expense of increased computational work to improve the estimation accuracy for a nonlinear system with strong nonlinearity.

The following flaws remain in current popular state-estimation approaches. The EKF performs effectively in ''mild'' nonlinear environments. When a system is strongly nonlinear, the EKF tends to have poor estimation accuracy and even diverges because of the inevitable linearization errors during the calculation of the Jacobian matrix. Although the UKF performs well in nonlinear systems, it cannot be used in high-dimensional systems because of the numerical stability problem [22]. Both the EKF and UKF can suffer from the curse of dimensionality, and the effect of dimensionality may become harmful in high-dimensional state-space models with state vectors of size 20 or more, as mentioned in [23], especially when there is a high degree of nonlinearities in the equations that describe the state-space model, which is exactly the case for power systems. The state transition function in the UKF and CKF is often Holt's two-parameter linear smooth parameter prediction model, which involves parameter selection and has a substantial modeling error. The model and parameter constraints, as well as the computational overhead prevent the UKF and CKF from being centrally implemented for large-scale distributed systems. With nearly singular covariances or with virtually deterministic systems, CKF does not perform well. Because noise covariance matrices cannot be accurately predicted, CKF frequently encounters implementation issues in practice [24]. Cholesky factorizations may be incomplete if a good estimate of the noise covariance is not provided because of the uncorrelated received data (the posteriori error-covariance matrix is not positive/semipositive definite). Consequently, the estimation process can be halted. Although it requires more computational work, EnKF performs well in high-dimensional systems; however, its performance is constrained by strongly nonlinear applications that have finite ensemble sizes and high accuracy requirements [25]. As a result, there are still many unanswered questions regarding nonlinear Kalman filtering for highly dimensional, strongly nonlinear systems. The additive Gaussian noise assumption made by the EKF, UKF, CKF, and EnKF limits the use of these methods. As a result, they are not appropriate for studying probability distributions with multiple modes. The particle filter (PF), in contrast, is more applicable to highly nonlinear systems since it does not make the restrictive assumption.

Distribution systems often have a fairly small number of measuring devices, unlike transmission systems, which feature redundant measurements. Pseudo-measurements of the load node power injections with significant inaccuracies are typically used to ensure observability. The fact that a significant portion of a distribution system is still unmonitored or that even when monitored, data are not transmitted for real-time monitoring and control because of communication limitations, such as high bandwidth requirements and privacy concerns [26], is one of the most significant challenges for state estimation in a distribution context. Real measurements in a distribution system are typically insufficient to implement state estimation [29], despite the fact that academics have offered a variety of strategies for installing limited meters in a distribution system [27], [28].

Phasor-measurement units (PMUs) are widely used in distribution systems. Distribution systems have fewer sensors and measurements than transmission systems and, because of their extensively dispersed and varied infrastructure, distribution networks can experience greater measurement uncertainties [30]. Field data from phasor measurement units (PMUs) are frequently tainted using colored and non-Gaussian noise [31]. According to research conducted by the Pacific Northwest National Laboratory (PNNL), PMU measurement noise exhibits a non-Gaussian heavy-tailed distribution [32], [33]. When unexpected noise pollutes the measurements, resulting in heavy-tailed measurement noise, the estimation accuracy of filters based on Gaussian assumptions degrades [34].

Nonlinear KF have been used in distribution systems for many years; however, addressing high-dimensional and strongly nonlinear non-Gaussian noise estimation problems remains a challenge. To cope with complicated and nonlinear distribution systems exhibiting substantial non-Gaussian uncertainties, a computationally efficient and accurate DSE technique is required [34].

In this study, to obtain the dynamic states with sufficient accuracy to deal with model nonlinearity and meet real-time demand, we focused on applying the Koopman operator theory to resolve the DSE problem of distribution systems. This study presents the first application of Koopman operator theory to the state estimation of a distribution system.

To address the above problems, KKPF, a data-driven DSE method based on the Koopman operator theory that does not rely on the power system model, is proposed. Compared with existing methods, the KKPF has the following advantages:

1) There are two key benefits to using the Koopman operator: First, as opposed to the pointwise description using orbits, it provides a comprehensive view of the system. Second, as it is a linear operator, it offers a linear approach to the (nonlinear) systems. The Koopman operator provides a global description of nonlinear dynamic systems in terms of the evolution of observable functions of the state space. The Koopman operator is a powerful tool that can be used to linearize nonlinear systems in the large [35].
2) The Koopman observer form (KOF) is linear, enabling the use of Kalman-like linear observers for nonlinear estimation. A notable property of KKPF using KOF is that it can be pursued directly from data, but does not require an underlying model. The KKPF has a good prediction ability and strong tracking ability because it is utilized to replace the distribution system model, which considerably decreases the error generated by the traditional method owing to linearization. Furthermore, the KPPF may produce good estimation results even with a small number of measuring devices. As a result, the KKPF is appropriate for power distribution systems with a limited number of measurement devices; therefore, the proposed method is acceptable for dynamic state estimation in large distribution systems.
3) Using a kernel-based extended dynamic mode decomposition (EDMD) approach, DSE based on the Koopman operator theory can be applied to high-dimensional systems. Therefore, the proposed method is acceptable for dynamic state estimation in large distribution systems.
4) KKPF combines the Koopman Kalman filter (KKF) with the PF to accurately estimate the dynamic states of distribution systems. KKPF offers a high estimation accuracy for high-dimensional nonlinear and non-Gaussian systems, such as complex distribution systems. Through simulation experiments, we found that KKPF is effective for distribution system state estimation with more pseudo -measurements and fewer real-time measurements.

The remainder of this paper is organized as follows. Section II reviews the fundamental concepts of Koopman operator theory and introduces a framework for Koopman operator-based observer synthesis. In Section III, the KKPF is proposed. Section IV details the simulation based on the IEEE 141 system and corresponding analyses. Finally, Section V presents the conclusions of this study.

II. PRELIMINARIES

In this section, the general dynamic model of a distribution system is firstly described. Then, a novel data-driven distribution system model based on the Koopman operator is constructed, which can facilitate the estimator design. Table 1 presents the notations used in the distribution system model.

TABLE 1. Distribution system model notations.

Symbol	Description
V	Voltage amplitude
δ	Voltage phase angle
$\boldsymbol{x}$	States of distribution system, including voltage amplitude and voltage phase angle
$\boldsymbol{f}$	Process function
$\boldsymbol{zm}$	Measurement value
$\boldsymbol{h}$	Measurement function
$\boldsymbol{w}$	Noise vector of the process model
$\boldsymbol{e}$	Measurement noise
$\boldsymbol{Q}$	Covariance matrices of $\boldsymbol{w}$
$\boldsymbol{R}$	Covariance matrices of $\boldsymbol{e}$
k	Time instant
$\widetilde{\boldsymbol{x}}$	Prediction state
$\widehat{\boldsymbol{x}}$	Estimation state
$\mathcal{K}$	Koopman operator
ψ	Vector-valued functions
$\boldsymbol{g}$	Full-state observable function
λ	Eigenvalue of the Koopman operator
$\boldsymbol{\varphi}$	Eigenfunction of the Koopman operator
$\boldsymbol{v}^x$	Modes for full-state observables $\boldsymbol{g}$
$\boldsymbol{v}^h$	Modes for any other observables $\boldsymbol{h}$
$\boldsymbol{\Psi}$	Koopman eigenfunctions, a vector-valued function
$\mathbf{X}$, $\mathbf{Y}$	Data set of states of the distribution system
$\boldsymbol{H}_X$	Data set of measurements of the distribution system
$\boldsymbol{\Psi}_X$, $\boldsymbol{\Psi}_Y$	Data set of states of the distribution system
K	Finite-dimensional approximation of $\mathcal{K}$
$\boldsymbol{\xi}$	Right eigenvectors of K
$\boldsymbol{z}$	Lifted state
$\boldsymbol{A}$, $\boldsymbol{C}^h$, $\boldsymbol{C}^x$	Coefficient matrices of the Koopman observer form

A. DSE MODEL OF THE DISTRIBUTION SYSTEM

The mathematical model for the DSE comprises the following process and measurement equations:

$$\begin{cases} \boldsymbol{x}_k = \boldsymbol{f}(\boldsymbol{x}_{k-1}) + \boldsymbol{w}_k \\ \boldsymbol{zm}_k = \boldsymbol{h}(\boldsymbol{x}_k) + \boldsymbol{e}_k \end{cases}, \tag{1}$$

where $\boldsymbol{x}_k = [\boldsymbol{V}^T; \boldsymbol{\delta}^T]^T \in R^d$ denotes a state vector in the distribution system, $\boldsymbol{x}_k$ and $\boldsymbol{x}_{k-1}$ denote the system state at times k and $k-1$, respectively, $\boldsymbol{f}(\boldsymbol{x})$ represents the process function describing the dynamic system, $\boldsymbol{h}(\boldsymbol{x})$ denotes the measurement function, $\boldsymbol{w}_k$ and $\boldsymbol{e}_k$ represent the noise vector and measurement noise of the process model, respectively, and k represents time. $\boldsymbol{f}(\boldsymbol{x})$ and $\boldsymbol{h}(\boldsymbol{x})$ are generally nonlinear, and $\boldsymbol{w}_k$ and $\boldsymbol{e}_k$ are typically assumed to be independent Gaussian white noise in $\begin{cases} \boldsymbol{w}_k \sim N(0, \boldsymbol{Q}_k) \\ \boldsymbol{e}_k \sim N(0, \boldsymbol{R}_k) \end{cases}$, where $\boldsymbol{Q}_k$ and $\boldsymbol{R}_k$ are the system and measurement noise variance, respectively.

The composition of the measurements for each node is as follows.

$$\boldsymbol{zm}_k = [V_i, \delta_i, P_i, Q_i, P_{ij}, Q_{ij}]^T, \tag{2}$$

where P_i and Q_i denote the injected active and reactive powers of the node, P_{ij} and Q_{ij} represent the active and reactive power flows of the branch, respectively.

A widely used DSE method is the EKF, which is applicable to linear models. It is assumed that the mean remains constant because the states of the power system barely change during consecutive time steps. Therefore, (1) becomes

$$\widetilde{\boldsymbol{x}}_{k+1} = \widehat{\boldsymbol{x}}_k, \tag{3}$$

$$\boldsymbol{zm}_k = \boldsymbol{H}_k \boldsymbol{x}_k + \boldsymbol{e}_k, \tag{4}$$

where $\boldsymbol{H}_k$ denotes the measurement matrix at time k.

The basic DSE model is a traditional linear model as described above. However, the distribution system is complicated, and its topologies and power loads frequently change. Because precise, nonlinear distribution–system process models are difficult to obtain, we used the Koopman operator to estimate the dynamic states of a distribution system. The main concept of the KOF is to use power flow data to find the transition and observation matrices, which require only minimal model assumptions, and recover the system model from the observations in a data-driven manner, which could improve our ability to anticipate and regulate such systems.

B. KOOPMAN OPERATOR THEORETIC

In this section, we provide a brief overview of the theoretical concept of the Koopman operator [36]. For a nonlinear dynamic system given by (1), $\boldsymbol{x}_k \in \mathcal{M} \subset R^d$ and the state-transition function $\boldsymbol{f}(\cdot)$ which describes the nonlinear state evolution map the state space $\mathcal{M}$. Let $\mathcal{F}$ be space of *observables*, we define a vector-valued functions as $\psi: \mathcal{M} \to \mathbb{C}$ (where $\mathbb{C}$ denotes the complex plane) for the state space $\psi \in \mathcal{F}$. The Koopman operator $\mathcal{K}$ is a linear operator $\mathcal{K}: \mathcal{F} \to \mathcal{F}$ that maps ψ into a new function $\mathcal{K}\psi$:

$$(K\psi)(\boldsymbol{x}_k) = (\psi \circ \boldsymbol{f})(\boldsymbol{x}_k) \tag{5}$$

where $\circ$ denotes the composition of ψ with the $\boldsymbol{f}$.

Although dynamic system (1) is nonlinear and evolves in a finite-dimensional space, the Koopman operator $\mathcal{K}$ is linear but infinite-dimensional. The eigenvalue λ and eigenfunction $\boldsymbol{\varphi}$ of the Koopman operator, referred to as the *Koopman eigenvalues* (KEs) and *Koopman eigenfunctions* (KEFs), respectively, are defined as

$$\mathcal{K}\boldsymbol{\varphi} = \lambda\boldsymbol{\varphi}. \tag{6}$$

The set of all KEs, λ_j, $j = 1, 2, \cdots$ is called the point spectrum of the Koopman operator. The Koopman operator may also have residual and continuous parts of the spectrum, but the point spectrum was sufficient for our study. Notably, if $\boldsymbol{\varphi}_1, \boldsymbol{\varphi}_2$ are KEFs with eigenvalues of λ_1, λ_2, then $\boldsymbol{\varphi}_1\boldsymbol{\varphi}_2$ is also an eigenfunction with eigenvalue $\lambda_1\lambda_2$. From the relation

$$\boldsymbol{\varphi}(\boldsymbol{x}_k) = \boldsymbol{\varphi}(\boldsymbol{f}(\boldsymbol{x}_{k-1})) = \mathcal{K}\boldsymbol{\varphi}(\boldsymbol{x}_{k-1}) = \lambda\boldsymbol{\varphi}(\boldsymbol{x}_{k-1}), \tag{7}$$

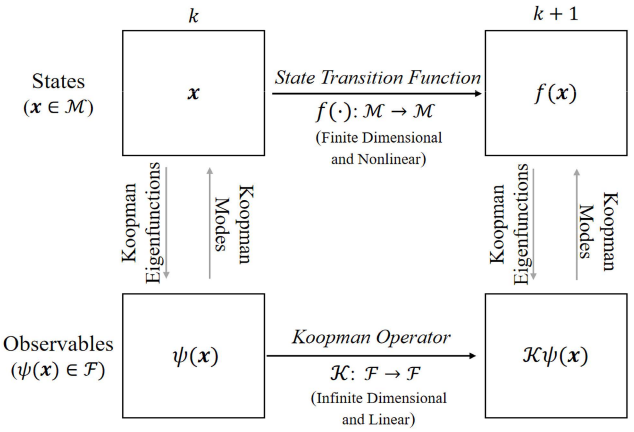

FIGURE 1. Koopman operator and its relation with the underlying dynamic system.

it follows that

$$\boldsymbol{\varphi}(\boldsymbol{x}_k) = \lambda^k \boldsymbol{\varphi}(\boldsymbol{x}_0). \tag{8}$$

The Koopman operator behaves multiplicatively in time compared with combinations of nonlinear maps, as shown in Fig. 1.

In Fig. 1, the *top path* depicts the evolution of states, $\boldsymbol{x}_k$, as a function of $\boldsymbol{f}(\boldsymbol{x})$, the *bottom path* updates the observables, $\psi \in \mathcal{F}$, using the Koopman operator, $\mathcal{K}$. Although f and $\mathcal{K}$ operate in distinct spaces, they encapsulate the same dynamics. The states and observables are connected through the full-state observable $\boldsymbol{g}(\boldsymbol{x}) = \boldsymbol{x}$. By writing $\boldsymbol{g}$ in terms of KEFs, we substitute the complex evolution of $\boldsymbol{x}$ with the straightforward linear evolution of $\boldsymbol{\varphi}_i$. To reconstruct $\boldsymbol{x}$, we superimpose the KEFs evaluated at a point that satisfies $(\mathcal{K}\boldsymbol{\varphi}_i)(\boldsymbol{x}_i) = \lambda_i\boldsymbol{\varphi}_i(\boldsymbol{x}_i)$, using the Koopman modes (KMs), as shown in (9). Consequently, both paths commute. One of the paths can solve either a finite-dimensional but nonlinear problem (the *top path*) or an infinite-dimensional but linear problem (the *bottom path*) if the KEs, KEFs, and KMs can be computed.

For the state equation of the distribution system, appropriately explaining the evolution of the state quantity becomes more difficult as the nonlinearity of the distribution system increases. It is easy and useful to calculate state $\boldsymbol{x}$ using the bottom path to estimate the states of the distribution system.

Now, consider the vector-valued observable $\boldsymbol{g}: R^d \to R^m$. If each of the m components of $\boldsymbol{g}$ lies within the span of KEs, $\boldsymbol{g}$, i = 1, 2, . . ., then $\boldsymbol{g}$ can be expanded in terms of these KEs as:

$$\boldsymbol{g}(\boldsymbol{x}_k) = \sum\nolimits_{i=1}^{\infty} \boldsymbol{\varphi}_i(\boldsymbol{x}_k)\boldsymbol{v}_i, \tag{9}$$

where $\boldsymbol{v}_i \in \mathbb{C}^m$ denotes the complex valued vectors. Using (8), the time evolution $\boldsymbol{g}(\boldsymbol{x}_k)$ can be expressed as

$$\boldsymbol{g}(\boldsymbol{x}_k) = \sum_{i=1}^{\infty} \lambda_i^k \boldsymbol{\varphi}_i(\boldsymbol{x}_0)\boldsymbol{v}_i. \tag{10}$$

We refer to this expansion as the KM decomposition (KMD) [37], where $\boldsymbol{v}_i$ represents the KMs associated with the eigenfunction $\boldsymbol{\varphi}_i$ and observable $\boldsymbol{g}$. These modes capture the correlations between the observable components, whereas the corresponding eigenvalue defines the growth/decay rates and oscillation frequencies of the modes. If the dynamics contain only a finite number of discrete spectra (peaks) in a complex plane, then a finite truncation of the expansion (10) yields a good approximation of the dynamics. KMD can be considered a generalized Fourier analysis and offers several advantages over the discrete Fourier transform [38]. Each KM represents only one frequency component and is thus expected to decouple the dynamics at different time scales more effectively than a proper orthogonal decomposition [39].

Notably, although KEs/KEFs are intrinsic to the dynamics (1), the modes depend on the choice of the observable $\boldsymbol{g}$. Modes $\boldsymbol{v}^x$ for full-state observables $\boldsymbol{g}(\boldsymbol{x}) = \boldsymbol{x}$ are referred to as KMs, whereas the modes $\boldsymbol{v}^h$ for any other observables $\boldsymbol{h}(\boldsymbol{x})$ are referred to as output KMs (OKMs). KMs are defined with respect to the KEFs associated with specific dynamics; therefore, they also capture information on the underlying dynamics [40]. Finally, we refer to the KEs, KEFs, and KMs $(\lambda_i, \boldsymbol{\varphi}_i, \boldsymbol{v}_i)$ as *Koopman tuple*. We adopted the EDMD algorithm [41] to compute the Koopman tuple, which we found to be suitable for power-system applications [42], and discuss it in further detail in Section II C. This is an equation-free approach that relies on time traces/snapshots of appropriate observables generated from the system (1).

C. KOOPMAN OBSERVER FORM

In this section, we briefly overview KOF (please refer to [43] for more details). We summarize the EDMD approach [44] and its kernel version [45], which we used for Koopman tuple computation to obtain the KOF. EDMD is a Galerkin-weighted residual approach that uses a dictionary of observable functions to approximate KEFs and corresponding KEs. It involves nonlinear maps, which are often heuristically predetermined, of the data (e.g., radial observable functions, monomials, or Gaussian functions) to capture the nonlinearity of dynamics. The EDMD procedure has two prerequisites: (1) a dataset of snapshot pairs, that is, $\{(\boldsymbol{x}_i, \boldsymbol{y}_i)\}_{i=1}^{M}$, organized as a pair of datasets, and (2) a vector of observable functions, $\mathcal{D} = \{\psi_1, \psi_2, \cdots, \psi_D\}$, $\mathcal{F}_D \subset \mathcal{F}$.

Remark: The choice of observable functions is critical. To depict the eigenfunctions of the Koopman operator better, a set of generally complete observable functions must be used as observable measurements of an operator action. Meanwhile, the selection of localized functions is required to characterize the distribution and identify the evolution of various phase-space points.

In this study, we assumed that the snapshots were evenly sampled; however, this was generally not required [44], [45]. The data matrices are defined as:

$$\boldsymbol{X} = [\boldsymbol{x}_1, \boldsymbol{x}_2, \cdots, \boldsymbol{x}_M], \quad \boldsymbol{Y} = \left[\boldsymbol{y}_1, \boldsymbol{y}_2, \cdots, \boldsymbol{y}_M\right], \tag{11}$$

$$\boldsymbol{H}_X = [\boldsymbol{h}(\boldsymbol{x}_1), \boldsymbol{h}(\boldsymbol{x}_2), \cdots, \boldsymbol{h}(\boldsymbol{x}_M)], \tag{12}$$

where $\boldsymbol{x}_i$ and $\boldsymbol{y}_i$ denote snapshots of the system state with $\boldsymbol{y}_i = \boldsymbol{f}(\boldsymbol{x}_i)$ and $\boldsymbol{h}(\boldsymbol{x}_i)$ is measurement data defined in (2). We also define the vector-valued $\boldsymbol{\Psi} : \mathcal{M} \to \mathbb{C}^{1\times D}$ as

$$\boldsymbol{\Psi}(\boldsymbol{x}_i) = [\psi_1(\boldsymbol{x}_i), \psi_2(\boldsymbol{x}_i), \ldots, \psi_D(\boldsymbol{x}_i)], \tag{13}$$

$$\boldsymbol{\Psi}_X \triangleq \begin{bmatrix} \boldsymbol{\Psi}(\boldsymbol{x}_1) \\ \boldsymbol{\Psi}(\boldsymbol{x}_2) \\ \vdots \\ \boldsymbol{\Psi}(\boldsymbol{x}_M) \end{bmatrix}, \quad \boldsymbol{\Psi}_Y \triangleq \begin{bmatrix} \boldsymbol{\Psi}(\boldsymbol{y}_1) \\ \boldsymbol{\Psi}(\boldsymbol{y}_2) \\ \vdots \\ \boldsymbol{\Psi}(\boldsymbol{y}_M) \end{bmatrix}. \tag{14}$$

$\boldsymbol{\Psi}_X$ and $\boldsymbol{\Psi}_Y$ are in $R^{M\times D}$.

Next, we generate K, a finite-dimensional approximation of $\mathcal{K}$. The K is given by

$$K \triangleq \boldsymbol{G}^{\dagger}\boldsymbol{A} \tag{15}$$

where $\boldsymbol{G} = \boldsymbol{\Psi}_X^T\boldsymbol{\Psi}_X$ and $\boldsymbol{A} = \boldsymbol{\Psi}_X^T\boldsymbol{\Psi}_Y$ denote $D \times D$ matrices and † represents the Moore-Penrose pseudoinverse [46]. Using the kernel trick, the entries of matrices $\boldsymbol{G}$ and $\boldsymbol{A}$ can be computed directly without forming $\boldsymbol{\Psi}(\boldsymbol{x})$ to compute the inner products of the form $\boldsymbol{\Psi}^T(\boldsymbol{x}_i)\boldsymbol{\Psi}(\boldsymbol{x}_j)$ as

$$\boldsymbol{G}_{ij} = Kernel\left(\boldsymbol{X}_i, \boldsymbol{X}_j\right), \quad \boldsymbol{A}_{ij} = Kernel\left(\boldsymbol{Y}_i, \boldsymbol{X}_j\right). \tag{16}$$

Let $\boldsymbol{\lambda}_i, i = 1, \ldots, D$ represent the eigenvalues of K with the corresponding right eigenvectors $\boldsymbol{\xi}_i$. Then, used $\boldsymbol{\xi}_i$ to approximate the KEs with the corresponding KEFs, given by

$$\boldsymbol{\Phi}_X = [\boldsymbol{\varphi}_1, \boldsymbol{\varphi}_2, \cdots, \boldsymbol{\varphi}_D] = \boldsymbol{\Psi}_X[\boldsymbol{\xi}_1, \boldsymbol{\xi}_1, \cdots, \boldsymbol{\xi}_D]. \tag{17}$$

Then, the KMs can be obtained using

$$\boldsymbol{v}^x = [\boldsymbol{v}_1^x; \boldsymbol{v}_2^x; \cdots; \boldsymbol{v}_D^x] = (\boldsymbol{\Phi}_X)^{\dagger}X^T. \tag{18}$$

Let the coordinate function $\boldsymbol{g}(\boldsymbol{x}_k) = \boldsymbol{h}(\boldsymbol{x}_k)$ be in the span of $\mathcal{D}$ so that OKMs can be obtained via

$$\boldsymbol{v}^h = [\boldsymbol{v}_1^h; \boldsymbol{v}_2^h; \cdots; \boldsymbol{v}_D^h] = (\boldsymbol{\Phi}_X)^{\dagger}\boldsymbol{H}_X^T, \tag{19}$$

where $\boldsymbol{X}$ and $\boldsymbol{H}_X$ are defined using (11) and (12), respectively.

Let $\mathcal{F}^D = span\{\boldsymbol{\varphi}_i\}_{i=1}^{D}$ be a subset of KEFs for system (1), such that $\boldsymbol{h}(\boldsymbol{x}), \boldsymbol{x} \in F^D$; then,

$$\boldsymbol{x}_k = \sum_{i=1}^{D}\boldsymbol{\varphi}_i(\boldsymbol{x}_k)\boldsymbol{v}_i^x, \quad \boldsymbol{x}_{k+1} = \sum_{i=1}^{D}\lambda_i\boldsymbol{\varphi}_i(\boldsymbol{x}_k)\boldsymbol{v}_i^x \tag{20}$$

$$\boldsymbol{h}(\boldsymbol{x}_k) = \sum_{i=1}^{D}\boldsymbol{\varphi}_i(\boldsymbol{x}_k)\boldsymbol{v}_i^h, \quad \boldsymbol{h}(\boldsymbol{x}_{k+1}) = \sum_{i=1}^{D}\lambda_i\boldsymbol{\varphi}_i(\boldsymbol{x}_k)\boldsymbol{v}_i^h, \tag{21}$$

where $\boldsymbol{v}_i^x \in \mathbb{C}^d, i = 1, 2, \cdots, D$ denotes the KMs and $\boldsymbol{v}_i^h \in \mathbb{C}^m, i = 1, 2, \cdots, D$ represents the OKMs.

Notably, if λ is a complex KE with KEF $\boldsymbol{\varphi}$, then the complex conjugate $\overline{\lambda}$ is also a KE with KEF $\overline{\boldsymbol{\varphi}}$. Similarly, for real-valued observables $\boldsymbol{h}$, the KMs occur in conjugate pairs. Herein, we ordered KEFs $\{\boldsymbol{\varphi}_1, \boldsymbol{\varphi}_2, \cdots, \boldsymbol{\varphi}_D\}$ (and the corresponding KEs and KMs/OKMs) such that the complex conjugates appeared adjacent to each other. We use $\mathrm{Re}(\boldsymbol{\varphi})$ and $\mathrm{Im}(\boldsymbol{\varphi})$ to denote the real and imaginary parts of any complex number $\boldsymbol{\varphi} \in \mathbb{C}$, respectively.

A nonlinear change in the coordinates $\Gamma u(\boldsymbol{x}_k) = (\hat{\boldsymbol{\varphi}}_1(\boldsymbol{x}_k), \hat{\boldsymbol{\varphi}}_2(\boldsymbol{x}_k), \cdots, \hat{\boldsymbol{\varphi}}_D(\boldsymbol{x}_k))^T$ is defined as follows:

• $\hat{\boldsymbol{\varphi}}_i = \boldsymbol{\varphi}_i$ if the i th KEF is real and

• $\hat{\boldsymbol{\varphi}}_i = 2Re(\boldsymbol{\varphi}_i)$ and $\hat{\boldsymbol{\varphi}}_{i+1} = -2Im(\boldsymbol{\varphi}_i)$ if the ith and $i+1$th KEFs are complex conjugate pairs.

Nonlinear changes in coordinates defined by $\Gamma u : R^d \rightarrow R^D$,

$$z_k = \Gamma u(\boldsymbol{x}_k). \tag{22}$$

We refer to this transformation as the Koopman canonical transform (KCT), and the coordinates $z_k = (z_{1,k}, z_{2,k}, \cdots, z_{D,k})^T \in R^D$ as the Koopman canonical coordinates (KCC).

Further, $z_k = \boldsymbol{A} z_{k-1}$, where $\boldsymbol{A}$ is a real $n \times n$ block diagonal matrix, such that

• $\boldsymbol{A}$ has a diagonal entry $\boldsymbol{A}_{i,i} = \lambda_i$ if the ith KEF is real, and

• $\boldsymbol{A}$ has a diagonal block entry $\begin{bmatrix} \boldsymbol{A}_{i,i} & \boldsymbol{A}_{i,i+1} \\ \boldsymbol{A}_{i+1,i} & \boldsymbol{A}_{i+1,i+1} \end{bmatrix} = |\lambda_i| \begin{pmatrix} \cos(\arg \lambda_i) & \sin(\arg \lambda_i) \\ -\sin(\arg \lambda_i) & \cos(\arg \lambda_i) \end{pmatrix}$ if the ith and $i+1$th KEFs are complex conjugate pairs.

Furthermore, KMD (11) can be expressed in terms of KCC as

$$\boldsymbol{x}_k = \boldsymbol{C}^x z_k, \quad \boldsymbol{h}(\boldsymbol{x}_k) = \boldsymbol{C}^h z_k, \tag{23}$$

where $\boldsymbol{C}^x \in R^{d \times D}$and $\boldsymbol{C}^h \in R^{m \times D}$ denote the matrices obtained from KMs and OKMs, respectively. For instance, the ith column of $\boldsymbol{C}^x$ is $(\boldsymbol{v}_i^x)^{\mathrm{T}}$ if the ith KEF is real, and the ith and $i+1$th columns of $\boldsymbol{C}^x$ are $\mathrm{Re}\,(\boldsymbol{v}_i^x)^{\mathrm{T}}$ and $\mathrm{Im}(\boldsymbol{v}_i^x)^{\mathrm{T}}$, respectively, if the ith and $i+1$th KEFs are complex conjugate pairs. A similar construction is applied to $\boldsymbol{C}^h$.

In summary, with z_k(KCC), the evolution of the full-state observable $\boldsymbol{x}_k$ and $\boldsymbol{h}(\boldsymbol{x}_k)$ can be expressed via a linear time-invariant system with the following outputs:

$$z_k = \boldsymbol{A} z_{k-1}, \tag{24}$$
$$\boldsymbol{zm}_k = \boldsymbol{h}(\boldsymbol{x}_k) = \boldsymbol{C}^h z_k, \tag{25}$$
$$\boldsymbol{x}_k = \boldsymbol{C}^x z_k. \tag{26}$$

In system (1), the state estimate is obtained by using a nonlinear transform. By contrast, in KOF, the state estimate can be obtained via a linear transform (26), thereby providing a computational advantage. Given the KOF, one can design a standard KF, as discussed in the Section III.

III. KKPF

The KKF is based on the KOF and uses Kalman-like linear observers for nonlinear estimation. The key idea here is to obtain both transition matrices (24) and observation matrices (25) using power flow data to replace $\boldsymbol{f}(\cdot)$ and $\boldsymbol{h}(\cdot)$ in system (1). This process involved two steps.

1) Prediction Step:

$$\tilde{z}_k = \boldsymbol{A} \hat{z}_{k-1}, \tag{27}$$
$$\tilde{P}_k = \boldsymbol{A} \hat{P}_{k-1} \boldsymbol{A}^T + \boldsymbol{Q}_k. \tag{28}$$

2) Correction (Filtering) Step:

$$\boldsymbol{K}_k = \tilde{P}_k (\boldsymbol{C}^h)^T [\boldsymbol{C}^h \tilde{P}_k (\boldsymbol{C}^h)^T + \boldsymbol{R}_k]^{-1}, \tag{29}$$
$$\hat{z}_k = \tilde{z}_k + \boldsymbol{K}_k [\boldsymbol{zm}_k - \boldsymbol{C}^h z_k], \tag{30}$$
$$\hat{\boldsymbol{P}}_k = \tilde{\boldsymbol{P}}_k - \boldsymbol{K}_k \boldsymbol{C}^h \tilde{\boldsymbol{P}}_k. \tag{31}$$

In (27)–(31), $\tilde{z}_k$ and $\hat{z}_k$ denote the predicted and filtered state vectors, $\widetilde{\boldsymbol{P}}_k$ and $\widehat{\boldsymbol{P}}_k$ represent the predicted and filtered state covariance matrices, respectively, $\boldsymbol{K}_k$ denotes the KF gain matrix, and $\boldsymbol{zm}_k \in R^m$ represents the measurement vector in canonical coordinates.

Then, we perform a KKF analysis to define the proposal density of a PF instead of the prior density, thereby reducing the risk of particle degeneracy. Considering that there are N initial ensembles $\left\{\boldsymbol{x}_{i,0}^a\right\}_{i=1}^N$, first, the ensembles are embedded through the inverse of the relation $\boldsymbol{x}_k = \boldsymbol{C}^x z_k$, and then the forecast ensembles $\left\{z_{i,k}^f\right\}_{i=1}^N$ are propagated through $z_k = \boldsymbol{A} z_{k-1}$ as

$$z_{i,k}^f = \boldsymbol{A} z_{i,k-1}^a. \tag{32}$$

Forecast ensembles were introduced into the KKF to calculate the Kalman gain using (29). Finally, the analysis particles are obtained using the following update procedure:

$$z_{i,k}^a = z_{i,k}^f + \boldsymbol{K}_k \left[\boldsymbol{zm}_{i,k} - \boldsymbol{C}^h \left(z_{i,k}^f\right) + \boldsymbol{R}_k\right], \tag{33}$$
$$\boldsymbol{x}_{i,k}^a = \boldsymbol{C}^x z_{i,k}^a, \tag{34}$$
$$\bar{\boldsymbol{x}}_k^a = \frac{1}{N} \sum_{i=1}^{N} \boldsymbol{x}_{i,k}^a. \tag{35}$$

In this study, a proposal density based on the mathematical model of distribution-system state estimation via the KOF analysis pdf was used. Suppose that the proposal density of each particle is a Gaussian density with a mean of $\boldsymbol{x}_{i,k}$ and covariance of $\widehat{\boldsymbol{P}}_k$, that is, $q(\boldsymbol{x}_{i,k} | \boldsymbol{x}_{i,k-1}, \boldsymbol{zm}_k) = N(\bar{\boldsymbol{x}}_{i,k}, \widehat{\boldsymbol{P}}_k)$, where $\bar{\boldsymbol{x}}_{i,t}$ represents the deterministic part of (33), that is,

$$\bar{\boldsymbol{x}}_{i,k} = \boldsymbol{C}^x (\boldsymbol{A} z_{i,k-1}^a + \boldsymbol{K}_k \left[\boldsymbol{zm}_k - \boldsymbol{C}^h \left(\boldsymbol{A} z_{i,k-1}^a\right)\right]. \tag{36}$$

In PF, the weight-updating formula is given by

$$\boldsymbol{w}_{i,k} = \boldsymbol{w}_{i,k-1} \frac{p\left(\boldsymbol{zm}_k \mid \boldsymbol{x}_{i,k}^a\right) p\left(\boldsymbol{x}_{i,k}^a \mid \boldsymbol{x}_{i,k-1}^a\right)}{q\left(\boldsymbol{x}_{i,k}^a \mid \boldsymbol{x}_{i,k-1}^a, \boldsymbol{zm}_k\right)}, \tag{37}$$

where the prior pdf $p(\boldsymbol{x}_{i,k}^a | \boldsymbol{x}_{i,k-1}^a)$ and likelihood pdf $p(\boldsymbol{zm}_k | \boldsymbol{x}_{i,k}^a)$ can be computed as

$$p\left(\boldsymbol{x}_{i,k}^a \mid \boldsymbol{x}_{i,k-1}^a\right) = N\left(\boldsymbol{C}^x \boldsymbol{A} \boldsymbol{z}_{i,k}^a, \widetilde{\boldsymbol{P}}_k\right), \tag{38}$$
$$p(\boldsymbol{zm}_k | \boldsymbol{x}_{i,k}^a) = N(\boldsymbol{C}^h \boldsymbol{z}_{i,k}^a, \boldsymbol{R}_k). \tag{39}$$

Thus, we can obtain the following weight-updating formula for the PF:

$$\boldsymbol{w}_{i,k} = \boldsymbol{w}_{i,k-1} \frac{N(\boldsymbol{C}^h \boldsymbol{z}_{i,k}^a, \boldsymbol{R}_k) * N(\boldsymbol{C}^x (\boldsymbol{A} \boldsymbol{z}_{i,k}^a, \widetilde{\boldsymbol{P}}_k))}{N(\bar{\boldsymbol{x}}_{i,k}, \widehat{\boldsymbol{P}}_k)}. \tag{40}$$

We resampled each time $N_{eff} = \frac{1}{\sum_i^N (\boldsymbol{w}_{i,k})^2}$ dropped below a given N_{thr}. The resampling threshold for $N_{thr} = N/2$ is generally chosen for PFs [47]. The residual resampling method

was used in this study. After the resampling process, all the particles are assigned the same weight, that is, $\boldsymbol{w}_{i,k} = 1/N$. The final estimated state is computed as follows:

$$\widehat{\boldsymbol{x}}_k = \sum_{i=1}^{N} \boldsymbol{w}_{i,k}^a \boldsymbol{x}_{i,k}^a. \tag{41}$$

Based on the aforementioned introduction, a schematic of the KKPF is shown in Fig. 2. The experimental procedure is summarized as follows:

1) Input dataset with snapshot pairs $\{(\boldsymbol{X}, \boldsymbol{Y})\}$ (11) and $\boldsymbol{H}_X$ (12).
2) Compute KEFs $\{(\lambda_i, \boldsymbol{\varphi}_i, \boldsymbol{v}_i)\}_{i=1}^N$ and OKMs $\{\boldsymbol{v}_i^h\}_{i=1}^N$ using (15)–(19).
3) $\boldsymbol{z}_0 = \Gamma u(\boldsymbol{x}_0)$ can be obtained directly from the last column of KCT (22). Equation (25) can also be inverted to obtain $\boldsymbol{z}_0 \approx (\boldsymbol{C}^h)^\dagger \boldsymbol{z}\boldsymbol{m}_k$.
4) At the initial time step $k = 0$, N particles with equal weights are generated from the prior pdf of the state variable: $\{\boldsymbol{x}_{i,0}\}_{i=1}^N \sim p(\boldsymbol{x}_0)$, $\{\boldsymbol{w}_{i,0}\}_{i=1}^N = 1/N$.
5) The particles are propagated using (32), and the forecast particles $\boldsymbol{z}_{i,k}^f\}_{i=1}^N$ are obtained.
6) Using (27)–(31), we used the measurement to update the forecast particles.
7) We can find the state vector using (26) and then obtain the analysis particles $\boldsymbol{x}_{i,k}^a\}_{i=1}^N$ employing by (33)–(35).
8) The updated weights $\boldsymbol{w}_{i,k}$ are calculated using (40).
9) If particle degeneracy occurs, residual resampling is performed for all particles. Otherwise, skip to step 11.
10) New particles with equal weights were generated using $\{\widetilde{\boldsymbol{w}}_{i,k}^a\}_{i=1}^N = 1/N$.
11) The final estimated state was calculated using (41).
12) If all the time steps are completed, the entire process stops. Otherwise, increment k by one and return to Step 5.

IV. CASE STUDIES

A. IMPLEMENTATION

1) OBSERVABLE FUNCTION SELECTION

In this study, we used $M = 7$ power flow snapshot pairs to compute the Koopman tuples $\{\lambda_i, \boldsymbol{\varphi}_i, \boldsymbol{v}_i\}$. The dataset comprises seven historical data trajectories for the previous seven sample sites. After running the simulations, we observed that the value of M is not always a good indicator of accurate estimation results. In fact, increasing M does not always improve the estimation accuracy; it may even decrease estimation accuracy when the value of M reaches a certain value. Seven sample sets are the minimum that can yield an accurate estimation based on the three observable functions selected according to our repeated simulations. The number of required historical datasets may vary if the simulations are run from different initial points but not considerably. KOF (24)–(26) can be designed using the dataset described in section II C. Then, $(\boldsymbol{A}, \boldsymbol{C}^x, \boldsymbol{C}^h)$ for KOF can be obtained.

It is crucial to select the correct observable function; however, there is no established method for this purpose. Thus, in this study, the observable function is selected through trial and error. The number of observable functions is 1000, which yields the formula $\mathcal{D} = \{\psi_1, \psi_2, \cdots, \psi_{1000}\}$. The thin-plate spline radial basis function (42), Gauss basis function (43), and polynomial basis function (44) are the three common observable functions in the literature that are compared in this study.

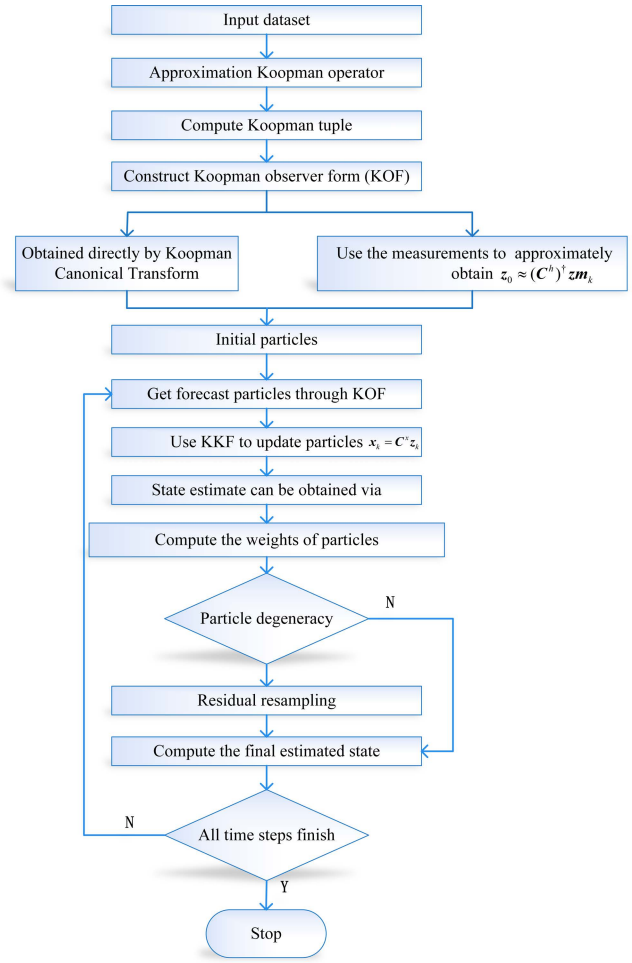

FIGURE 2. Schematic of the algorithm of the KKPF.

$$\psi_i(\boldsymbol{x}) = \|\boldsymbol{x} - \boldsymbol{x}_i\|^2 * \log(\|\boldsymbol{x} - \boldsymbol{x}_i\|), \quad i = 1, \cdots, D, \tag{42}$$

$$\psi_i(\boldsymbol{x}) = e^{-\|\boldsymbol{x} - \boldsymbol{x}_i\|}, i = 1, \cdots, D, \tag{43}$$

$$\psi_i(\boldsymbol{x}) = p^{\alpha_i} v^{\beta_i} u, i = 1, \cdots, D, \tag{44}$$

where $\boldsymbol{x}_i$ denotes the center and is selected randomly with a uniform distribution in the unit box, α_i and β_i represent the nonnegative integers, and i tabulates all combinations such that $\alpha_i + \beta_i \leq Q$, and $Q > 1$ define the largest allowed polynomial degree.

The accuracy of the estimations generated by each of the obtained KOFs of the KKPF was evaluated by comparing the power flow of the system to select the proper observable function. Fig. 3 compares the voltage amplitude estimates of the KKPFs using the three observable functions. The estimation inaccuracy is shown in Figs. 4 and 5 presents the average

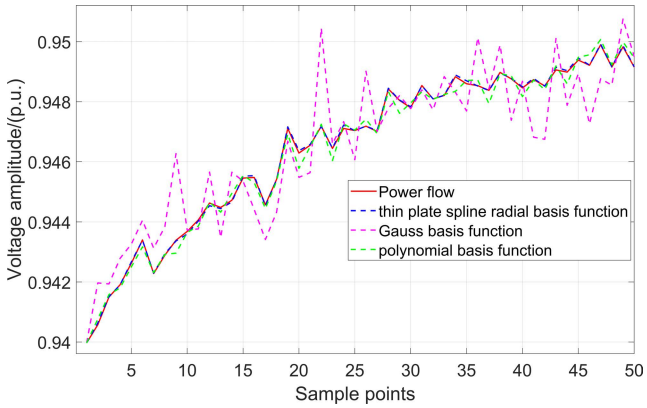

FIGURE 3. Voltage amplitude estimated via the KKPF using the three observable functions (example at node 15 in the IEEE 141 test system).

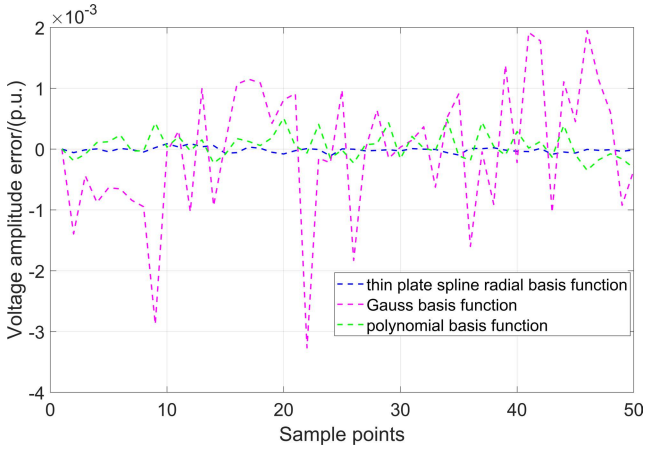

FIGURE 4. Voltage amplitude estimation error of the KKPF using the three observable functions (example at node 15 in the IEEE 141 test system).

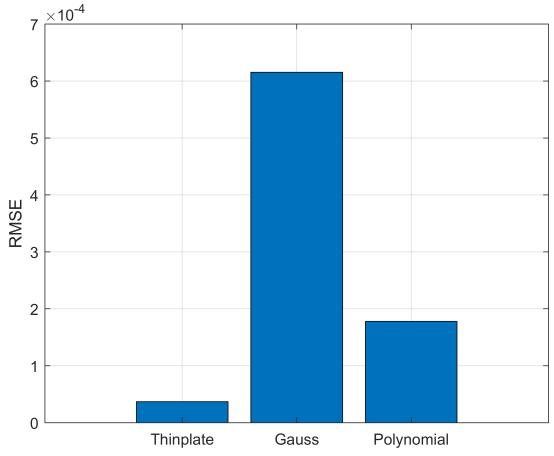

FIGURE 5. Average RMSE for the estimation comparison of the KKPF using the three observable functions (IEEE 141 test system).

root-mean-square errors (RMSEs) of the KKPFs based on the three functions.

Notably, the choice of observable functions for power systems (in general) [48], [49] remains an open problem

TABLE 2. Performance index under different particle numbers in the IEEE 141 test system.

Number of Particle		Amplitude relative error (%)		Phase angle absolute error (rad)	
		Avg	Max	Avg	Max
10	PF	0.3880	2.0919	0.0179	0.1210
	KKPF	0.0083	0.1823	0.00068	0.0148
20	PF	0.3202	1.3993	0.0148	0.0809
	KKPF	0.0053	0.0551	0.00054	0.0084
30	PF	0.3090	1.1823	0.0143	0.0684
	KKPF	0.0039	0.0160	0.00029	0.0011

and is beyond the scope of this study. Figs 3-5 show that the estimated voltage amplitude obtained using the thin-plate spline radial basis function fits the real voltage amplitude of the distribution system well. Furthermore, the nonlinear characteristics of the distribution system are best approximated using this basis function.

2) PARTICLE NUMBER SELECTION

The lowest number of particles required to accurately estimate the states is used to determine the number of particles for each system node. Because the weighted particles in particle filtering represent the pdf of the dynamic state, the performance is a function of the number of particles utilized. Effective state estimation requires the selection of an appropriate number of particles. We conducted a simulation test on the IEEE 141 system to determine the number of particles. To evaluate the performance of KKPF methods with different numbers of particles, three particle sets (10, 20, and 30) were considered in non-Gaussian noise environments in this study. To show the estimation results, we carried out simulation tests with more than 50 sampling points, and took the estimation results of the following 20 consecutive points and compared the effects, as shown in Figs. 6 and 7. The relevant indices for different particle numbers are listed in Table 2.

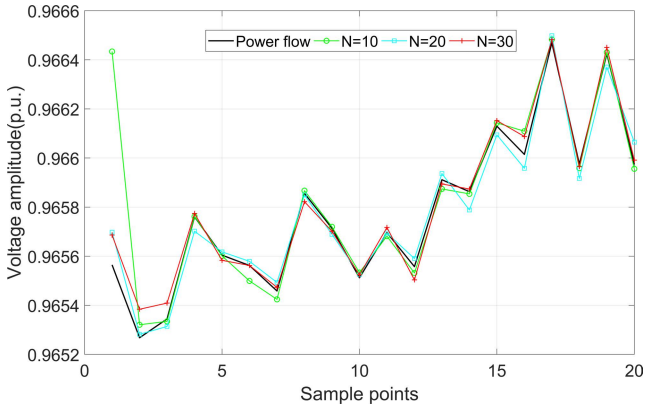

FIGURE 6. Voltage amplitude of the KKPF with respect to different numbers of particles.

With increasing numbers of particles, the KKPF method showed a slight tendency toward greater estimation accuracy.

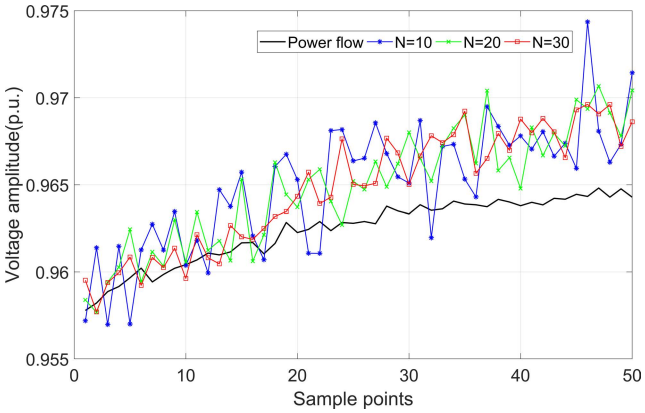

FIGURE 7. Voltage amplitude of the PF regarding different numbers of particles.

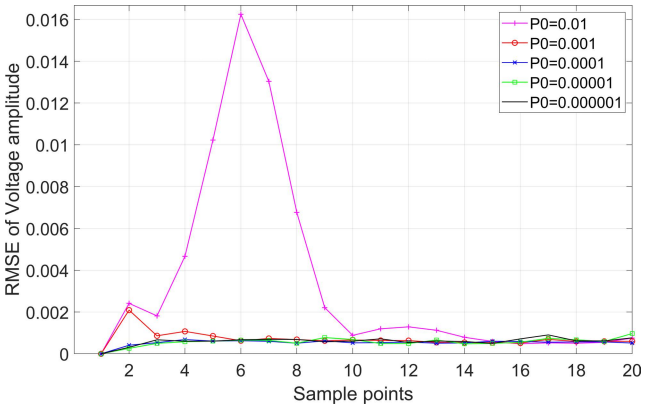

FIGURE 8. Impact of various values of P_0 on the convergence of the CKF (RMSE of voltage amplitude in the IEEE 141 test system).

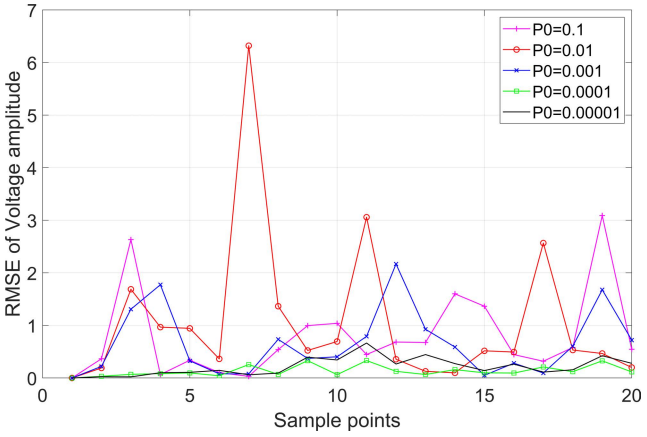

FIGURE 9. Impact of various values of P_0 on the convergence of the KPF (RMSE of voltage amplitude in the IEEE 141 test system).

Therefore, we chose 10 as the number of particles for the next simulation to reduce the running time and enhance practicality. The standard PF cannot produce an estimation as accurate as the KKPF. The simulation results suggest that the KKPF can provide accurate estimation results, thereby confirming its effectiveness.

3) SIZING IMPACT OF THE INITIAL VALUE OF STATE ERROR COVARIANCE

For comparison, various values of the diagonal elements of $\boldsymbol{P}_0$ were examined, ranging from 1×10^{-1} to 1×10^{-6} and the state error was obtained. To investigate the effect of $\boldsymbol{P}_0$ on the convergence of CKF, 20 sets of simulated measurement data were generated and used to run CKF with different $\boldsymbol{P}_0$ values. For the diagonal elements of $\boldsymbol{P}_0$, CKF caused severe divergence for a value of 1×10^{-1}. The solution converges, and the state estimation results are obtained for the diagonal elements of $\boldsymbol{P}_0$ with values of 1×10^{-2}, 1×10^{-3}, 1×10^{-4}, 1×10^{-5}, and 1×10^{-6}.

The initial value of the state error covariance matrix $\boldsymbol{P}_0$ plays an important role in the convergence of the CKF method, as shown in Fig. 8, but not in the convergence of the KKPF method, as shown in Fig. 9. The convergence of the CKF depends on the selection of the correct value of the state error covariance matrix $\boldsymbol{P}_0$.

In Fig. 8, for a value of 1×10^{-2} and the diagonal elements of $\boldsymbol{P}_0$, the peak is very high and a longer duration is required to settle at the steady-state value. For 1×10^{-4} and the diagonal elements of $\boldsymbol{P}_0$, the solution peak was almost nonexistent and settled quickly at the steady-state value. Hence, this value was used for the simulations of the IEEE 141 and improved 141 systems. Although a peak is observed in Fig. 9 when $\boldsymbol{P}_0 = 10^{-2}$, the value is very small and the RMSE at the peak is 10^{-4}, which still indicated a good estimation.

B. EXPERIMENTAL RESULTS AND ANALYSIS

This study adopts the IEEE 141 [50] test system and an improved 141 system for simulation experiments. The performances of the KKPF, EKF, CKF, and PF were compared and analyzed in the following three cases under different measurement environments: (1) the system noise and measurement noise were assumed to be Gaussian, (2) the system noise was considered to be Gaussian, whereas the measurement noise was assumed to be Laplacian, and (3) the measurement redundancy of the distribution system was changed.

To compare the performance of the different DSE methods, 50 consecutive sampling points were used in the three cases mentioned above for estimation. We assume that the measurements are redundant, and supervisory control and data acquisition (SCADA), PMU, and advanced metering infrastructure (AMI) data can be received at all sampling points. We assumed that the PMUs provide voltage and angle measurements at 60 fps. The PMU voltage amplitude measurement error had a standard deviation of 0.005 and mean value of 0. The calibration error of the PMU phase-angle measurement was 0.002, with a mean value of 0. The measurement error of the SCADA system has a standard deviation of 0.02 and a mean value of 0. Random Gaussian noise, $N(0, 0.02)$, is assumed for the system and measurement error, such that the covariance matrices $\boldsymbol{w}_k = diag\left(10^{-4}\right), \boldsymbol{e}_k = diag(10^{-4})$. The RMSE, mean relative error of voltage

amplitude, and maximum absolute error of voltage phase angle are the indices used for determining the relative accuracy of the proposed method. The initial conditions for the states of all nodes are determined by the power flow considering the steady-state behavior of all nodes and the active and reactive power data for all nodes based on the system data obtained from the MATPOWER toolbox [51].

1) ANALYSIS OF TEST RESULTS UNDER GAUSSIAN NOISE

a: IEEE 141 TEST SYSTEM

For the IEEE 141 test system, the PMUs are considered at nodes 1, 6, 8, 12, 15, 19, 21, 27, 28, 32, 34, 45, 49, 53, 56, 62, 75, 77, 80, 85, 86, 90, 94, and 102. Other nodes require SCADA to report measurement data. We assume that the pseudo-measurement information of the injected power of all nodes can be obtained using the AMI. The IEEE 141 test system is illustrated in Fig. 10. First, the distribution system operates normally, and the power flow is calculated using MATPOWER to obtain the state quantity, injected power at each node, and line power flow. Subsequently, the DSE method of the distribution system was verified by adding Gaussian white noise to the measurements.

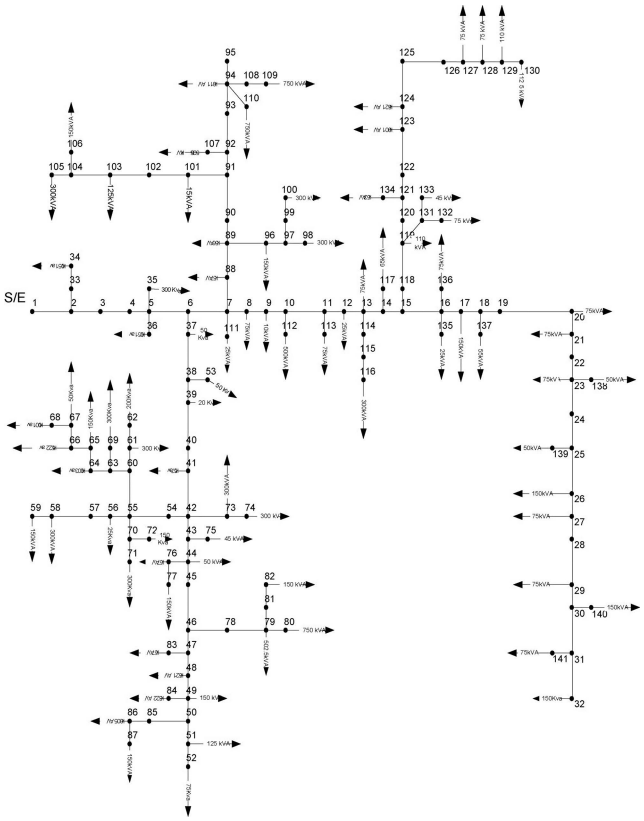

FIGURE 10. IEEE 141 test system.

To obtain consistent results from the simulations, the IEEE 141 test system was run 50 times with measurement values extracted randomly from the probability distribution of the measuring devices in each simulation. The relative error was

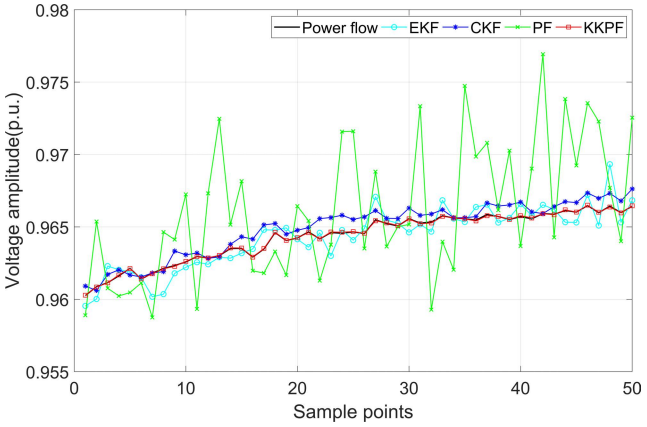

FIGURE 11. State-estimation results of voltage amplitude at node 58.

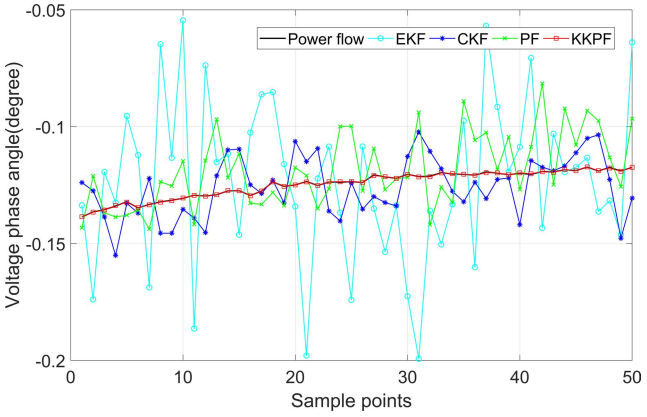

FIGURE 12. State-estimation results of voltage phase angle at node 58.

TABLE 3. Indices of different DSE methods in IEEE 141 system.

Filter Type	Amplitude relative error (%)		Phase angle absolute error (rad)	
	Avg	Max	Avg	Max
EKF	0.0698	0.4604	0.0291	0.3244
CKF	0.0682	0.2981	0.0080	0.0410
PF	0.2726	1.2577	0.0140	0.0714
KKPF	0.0024	0.0123	0.00022	0.00128

then calculated. Therefore, the state-estimation result provided in this study is the average outcome of the relative errors across the 50 simulations. The EKF, CKF, PF, and KKPF were run simultaneously, and the estimation results are shown in Figs. 11 and 12. The average estimation errors for the 50 simulations are compared with to the power flow of the IEEE 141 test system in Table 3. Table 3 shows that KKPF has the least error and is therefore more accurate than EKF, CKF, and PF. The variations in the relative values of the CKF and KKPF errors were of the order of 10^{-4} and 10^{-5}. The maximum relative error of the voltage amplitude for the CKF was on the order of 10^{-3}.The maximum relative error of the voltage amplitude for the KKPF was on the order of 10^{-4}.

However, the actual distribution system is a massive system with numerous nodes. We ran the simulation again in the later part with a larger node sample.

b: IMPROVED 141 SYSTEM

By adding branches to the IEEE141 system, we created a 246 system. The system diagram is displayed in Fig. 13. Do not multiply PMUs. Other nodes require SCADA to report measurement data. We assume that the pseudo-measurement information of the injected power of all nodes can be obtained using the AMI.

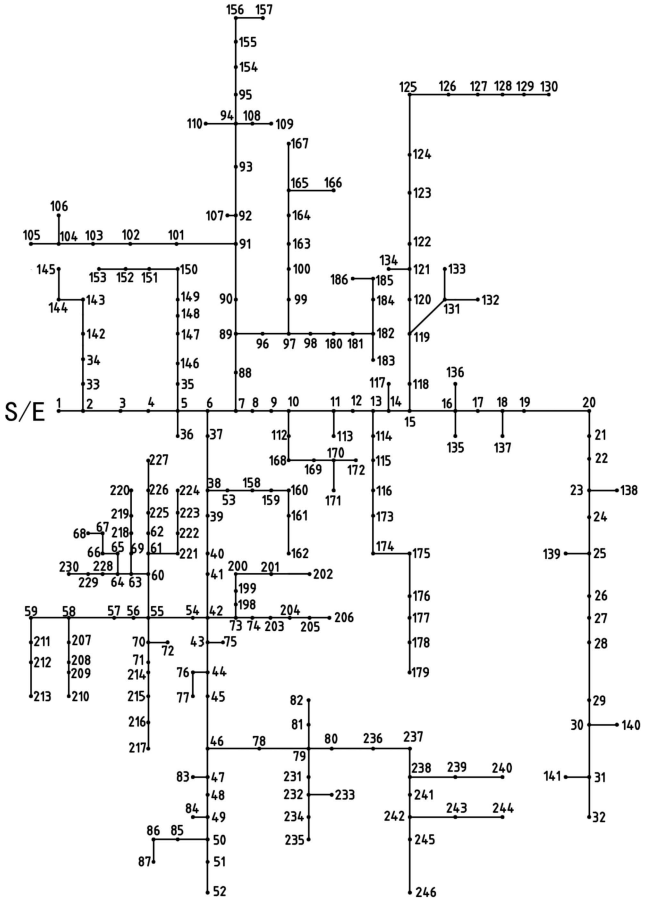

FIGURE 13. Improved 141 system.

The simulation outcomes obtained using the proposed KKPF technique were compared with those obtained using the EKF, CKF, and PF. To obtain consistent simulation outcomes, the simulation was performed 50 times, with measurement values randomly selected from the probability distribution of the measurement devices in each simulation. The estimation results of the voltage magnitude and angles at node 6 were compared in the line plot for 50 simulations of the observations, as shown in Figs. 14 and 15. The relevant indices are listed in Table 4.

The performance of the estimators is affected considerably as the system dimension increases, and all four methods

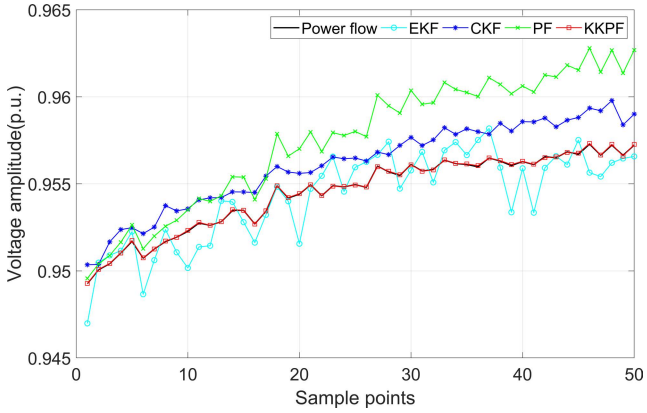

FIGURE 14. State-estimation results of voltage amplitude at node 58.

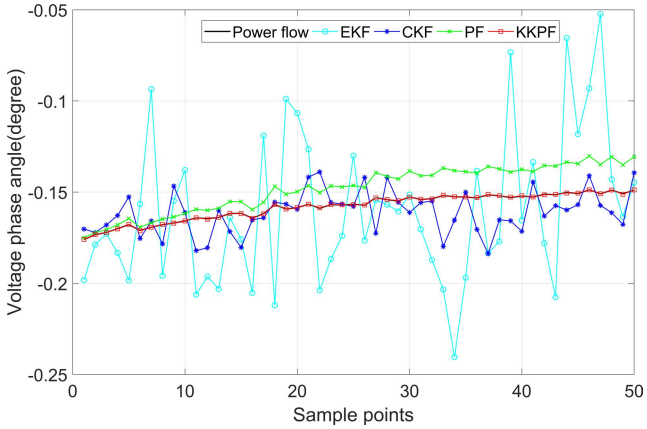

FIGURE 15. State-estimation results of voltage phase angle at node 58.

TABLE 4. Indices of different DSE methods in improved 141 system.

Filter Type	Amplitude relative error (%)		Phase angle absolute error (rad)	
	Avg	Max	Avg	Max
EKF	0.0940	0.6615	0.0382	0.3281
CKF	0.0801	0.3447	0.0101	0.0607
PF	0.3275	0.9940	0.0152	0.0576
KKPF	0.0031	0.0140	0.000245	0.001628

exhibit different levels of estimation deviations. In high-dimensional and highly nonlinear systems, this increases the estimation error (e.g., a distribution system involving trigonometric functions). The mean estimation error of CKF increased noticeably, as shown in Table 4. For example, the relative errors of the voltage amplitude of the EKF and CKF increased, and the outcome is variable compared with those of the IEEE 141 test system. Thus, the complexity of CKF increases linearly with the size of the stochastic system. In the case of high system state order, KKPF can achieve an ideal estimation effect. Therefore, when the ensemble size is sufficiently large, KKPF outperforms CKF in high-dimensional and highly nonlinear systems.

2) ANALYSIS OF TEST RESULTS UNDER NON-GAUSSIAN NOISE

For the DSE of a distribution system, measurement noise is assumed to follow a Gaussian distribution. However, in an actual distribution system, the high-permeability distributed energy increases the interference of the system, thus increasing the measurement noise and even non-Gaussian noise. The measurement noise of the distributed power supply is set to a Laplace distribution [32] created by performing the Laplace transform on a uniform distribution with the same mean and standard deviation as the Gaussian error.

The system noise, $\boldsymbol{w}$, was assumed to be Gaussian, and the measurement noise, $\boldsymbol{e}$, was assumed to be a Laplacian distribution. In many signal-processing problems, student-t and Laplace distributions are the two most widely used models for thick-tailed distributions, and can be used to simulate realistic PMU measurement errors [52].

The proposed KKPF was evaluated using improved 1 system to ensure good filtering under non-Gaussian measurement noise. The settings for the other parameters are the same as those used in the previous example. The estimation results of the three DSE methods are shown in Figs. 16 and 17.

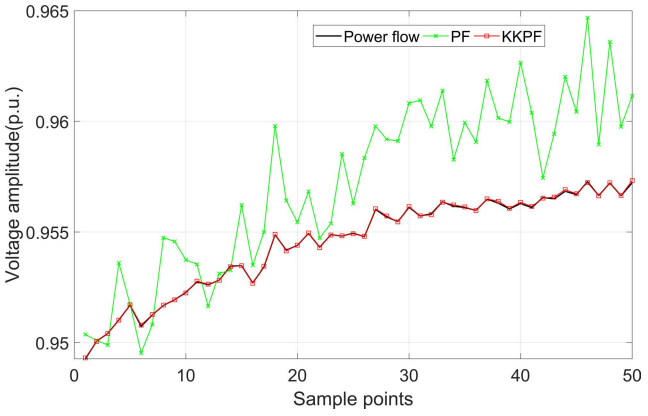

FIGURE 16. State-estimation results of voltage amplitude for node 58.

Figs. 16 show that when non-Gaussian measurement noise exists, KKPF can accurately track the true values of the voltage amplitude and phase angle. The KKPF retains the superior filtering capabilities of the traditional PF for non-Gaussian systems and uses the KKF to construct a proposal density function for the PF method, which overcomes PF particle deterioration. The average and maximum values of the relative voltage amplitude error and absolute voltage phase angle error for the two methods are reported in Table 5 to quantify the filtering performance.

According to the Table 4 and 5, whether the observed noise is Gaussian or non-Gaussian, the KKPF method performs better than the PF method. KKPF has high estimation accuracy for high-dimensional nonlinear and non-Gaussian systems.

TABLE 5. Performance index under non-gaussian noise.

Filter Type	Amplitude relative error (%)		Phase angle absolute error (rad)	
	Avg	Max	Avg	Max
PF	0.334295	1.018663	0.015479	0.059020
KKPF	0.003161	0.014649	0.000261	0.001666

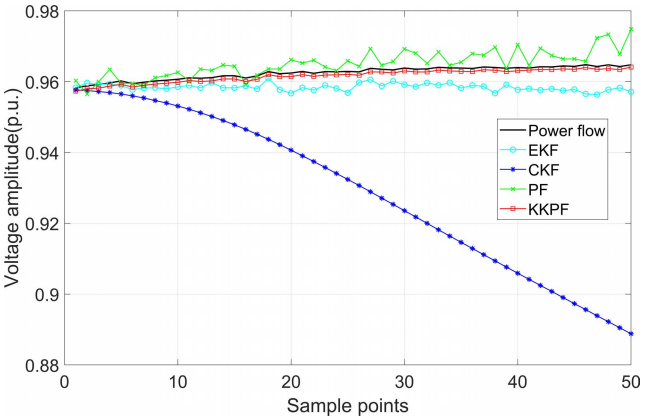

FIGURE 17. State-estimation results of voltage amplitude at node 6 under measurement for $h(x_k) = P_i^T$.

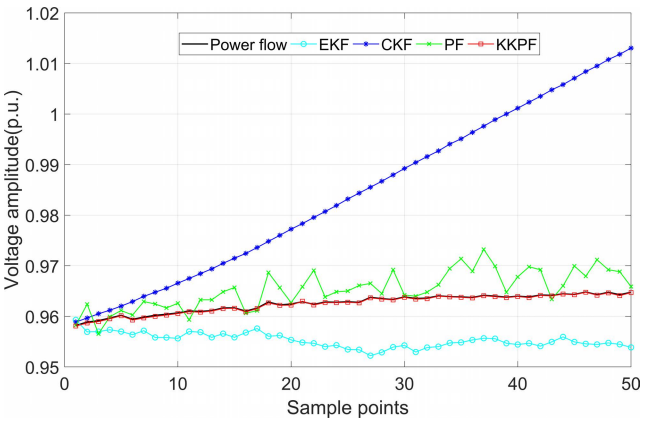

FIGURE 18. State-estimation results of voltage amplitude at node 6 under measurement for $h(x_k) = [P_i, Q_i]^T$.

3) ANALYSIS OF TEST RESULTS UNDER DIFFERENT MEASUREMENT REDUNDANCY

We discovered that the KKPF is more suitable for estimating the status of a distribution system when there are many pseudo-measurements and few real-time measurements. The goal of the Koopman operator is to recover a new data-driven representation for the distribution system that captures its inherent properties without additional model assumptions. Therefore, instead of nonlinear propagation of the measurements, the new representation can be linearly propagated and then lifted back to the measurement space [35]. Therefore, compared with existing methods, the KKPF can better grasp

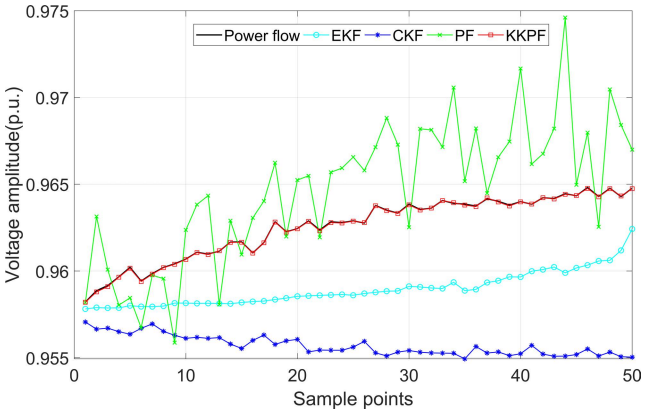

FIGURE 19. State-estimation results of voltage amplitude at node 6 under measurement for $h(x_k) = [P_i, Q_i, P_{ij}, Q_{ij}]^T$.

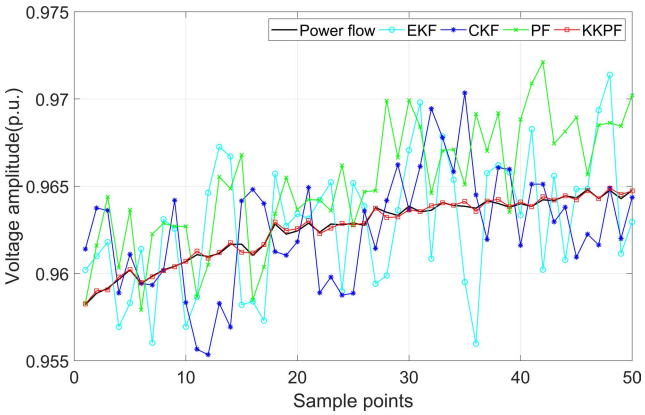

FIGURE 20. State-estimation results of voltage amplitude at node 6 under measurement for $h(x_k) = [V_{PMU}, \delta_{PMU}]^T$.

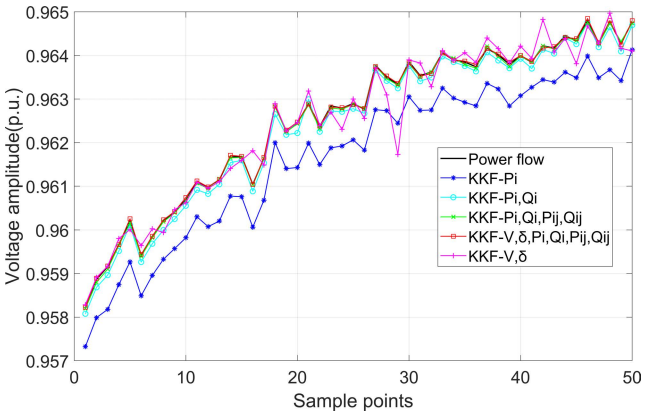

FIGURE 21. Comparison of KKPF estimation results for different measurements at node 6.

the dynamic characteristics of the system through quantitative measurements. First, we increased the quantity of pseudo-measurement and solely utilized them for correction; then, real-time measurements were added to compare the estimation outcomes of various methods in various measurement contexts. The estimation results are then simulated and tested using real-time PMU measurements. We used the improved 141 system to run the simulations described below. It is assumed that both the system and the measurement noise are Gaussian. In the simulation with increase pseudo-measurements, the measurement was increased from $\boldsymbol{h}(\boldsymbol{x}_k) = P_i^T$ to $\boldsymbol{h}(\boldsymbol{x}_k) = [P_i, Q_i]^T$, and then increased to $\boldsymbol{h}(\boldsymbol{x}_k) = [P_i, Q_i, P_{ij}, Q_{ij}]^T$. This process considerably affects the performance of the estimator. The estimation results are shown in Figs. 17-20. Fig. 21 shows a comparison of the voltage amplitudes of five different redundancy of the measurement at node 6.

In Figs. 17-20, by increasing the pseudo-measurements, KKPF can considerably ensure the accuracy of the estimation results compared with the other three methods, and it also has the maximum accuracy when only a few PMUs are observed in real time. However, we also discovered from the outcomes that KKPF still maintains a good estimation accuracy when compared to other methods, even when the pseudo-measurements are diminished, as in the case of missing data. Because the distribution system model is established based on the Koopman operator, the KKPF method can provide more accurate estimation results than the EKF and CKF methods when only a small number of measurements are available. Therefore, we believe that the KKPF is more appropriate for estimating the dynamic states of the distribution system.

4) RUNNING TIME COMPARISON

KKPF shows the best performance in estimating dynamic states. Because of the real-time requirement for estimating the dynamic states online, the run time of the dynamic state estimation method must be investigated. In the simulation of 50 sampling points on the improved 141 system, we compared the running times of EKF, CKF, and KKPF. The run times for EKF, CKF, PF, and KKPF is 10.761 s, 364.246 s, 364.246 s, and 338.555 s, respectively. It can be seen that the computation speed of KKPF is faster than CKF in high-dimensional systems. For the IEEE 141 system, the run times for EKF, CKF, PF, and KKPF is 0.979 s, 56.069 s, 56.503 s, and 143.144 s, respectively. The single computation time for the KKPF was 2.863 s, whereas the data sampling time for the current SCADA system for the power grid was 2∼4 s [53]. As a result, the computation time can still meet the real-time requirements of dynamic state estimation, even though KKPF requires the calculation of dimension augmentation.

The KKPF can also be used to estimate subregional states. The time consumed by the estimation can be reduced by the partition state estimation, which makes the method acceptable in practice. The procedure for building a KOF is simple and requires less time. Only embedding data and linear regression in a least-squares sense are needed to construct the KOF. Taking the IEEE 141 system as an illustration, the system is divided into two sub areas by disconnecting branch 10-11. Subsystems 1 and 2 were defined as the left and right areas, respectively. The states of the two sub-regions are estimated separately. The entire system was first subjected to

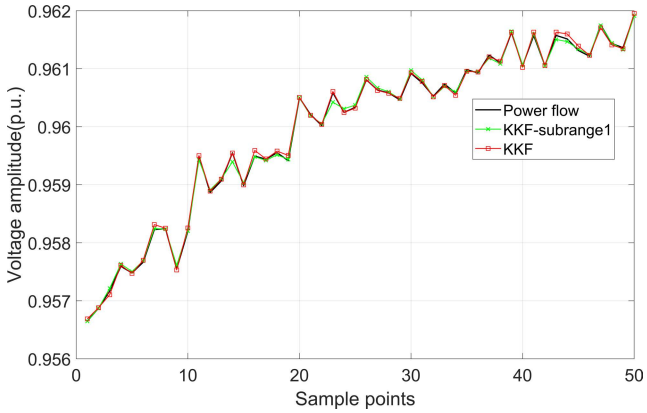

FIGURE 22. State-estimation results of voltage amplitude at node 10.

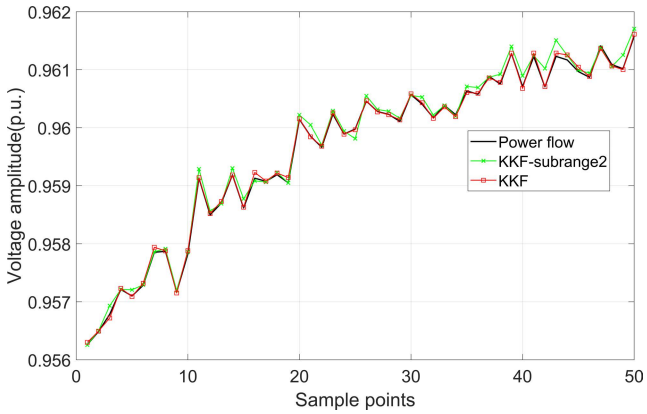

FIGURE 23. State-estimation results of voltage amplitude at node 11.

TABLE 6. Performance index of comparison estimation results between subregions and entire system.

Filter Type	Amplitude relative error (%)		Phase angle absolute error (rad)	
	Avg	Max	Avg	Max
subsyste1	0.001387	0.003842	0.00080	0.017964
subsyste2	0.002761	0.012513	0.001770	0.004327
entire system	0.002407	0.012343	0.000219	0.001280

a power flow simulation and computation. Take each linked node state quantity for the two subsystems, using the method introduced in Section 2. The voltage amplitudes determined by the two subsystems for nodes 10 and 11 are then compared to those of the original system.

The results of the state estimate for the subregion and those for the entire system differ only slightly, as shown in Figs. 22 and 23, and Table 6. It took 138.409 s for the KKPF to estimate the status of the 50 sample points in the entire system. It took 104.908 s for the KKPF to estimate the status of the 50 sample points in subsystem 1. In subsystem 2, the KKPF was used 73.396 s to assess the status of the 50 sample points. This time was significantly shortened after the division. Therefore, we believe that the KKPF is appropriate for measuring the states of a sub-region.

V. CONCLUSION

For the above problems of nonlinear increase in the distribution system, it is difficult to establish a distribution system model accurately, with few real-time measurements and non-Gaussian measurement noise; therefore, we propose a KKPF method for dynamic state estimation. The KKPF is an improved algorithmic kit that is a powerful tool for high-dimensional and highly nonlinear distribution systems.

The KKPF is data-driven and model-independent, has many potential applications, and achieves a high accuracy. Because the distribution system model is established based on the Koopman operator, the KKPF method provides more accurate estimation results than existing methods with a large number of pseudo-measurements and a small number of real-time measurements. This hybrid method, which takes full advantage of the strengths of the different theories, is likely to be applicable to complex distribution systems. Based on the simulation results, the KKPF produced more accurate simulation results when only a small number of measurements were available than the EKF, CKF, and PF. Therefore, the KKPF is suitable for distribution systems DSE and can improve its accuracy. Thus, it enhances the efficacy and practicality of DSE.

Dynamic state estimation based on Koopman theory can provide an accurate evaluation of the system state under the current distribution network configuration. It is necessary to investigate the Koopman dynamic state estimation technique because the KKPF state estimate conclusions are unreliable when a line fault occurs and the distribution network structure changes. Studying the robustness of the Koopman dynamic state estimation method for outliers is also necessary because KKPF may estimate more efficiently using a large number of pseudo-measurements.

REFERENCES

[1] A. P. S. Meliopoulos, G. J. Cokkinides, P. Myrda, Y. Liu, R. Fan, L. Sun, R. Huang, and Z. Tan, "Dynamic state estimation-based protection: Status and promise," in *IEEE Trans. Power Del.*, vol. 32, no. 1, pp. 320–330, Feb. 2017, doi: 10.1109/TPWRD.2016.2613411.

[2] Y. Liu, A. P. S. Meliopoulos, R. Fan, L. Sun, and Z. Tan, "Dynamic state estimation based protection on series compensated transmission lines," *IEEE Trans. Power Del.*, vol. 32, no. 5, pp. 2199–2209, Oct. 2017, doi: 10.1109/TPWRD.2016.2633410.

[3] J. Zhao, M. Netto, Z. Huang, S. S. Yu, A. Gomez-Exposito, S. Wang, I. Kamwa, S. Akhlaghi, L. Mili, V. Terzija, A. P. S. Meliopoulos, B. Pal, A. K. Singh, A. Abur, T. Bi, and A. Rouhani, "Roles of dynamic state estimation in power system modeling, monitoring and operation," *IEEE Trans. Power Syst.*, vol. 36, no. 3, pp. 2462–2472, May 2021, doi: 10.1109/TPWRS.2020.3028047.

[4] Y. Cui, R. G. Kavasseri, and S. M. Brahma, "Dynamic state estimation assisted out-of-step detection for generators using angular difference," *IEEE Trans. Power Del.*, vol. 32, no. 3, pp. 1441–1449, Jun. 2017, doi: 10.1109/TPWRD.2016.2615594.

[5] J. Zhao, J. Qi, Z. Huang, A. P. S. Meliopoulos, A. Gomez-Exposito, M. Netto, L. Mili, A. Abur, V. Terzija, I. Kamwa, B. Pal, and A. K. Singh, "Power system dynamic state estimation: Motivations, definitions, methodologies, and future work," *IEEE Trans. Power Syst.*, vol. 34, no. 4, pp. 3188–3198, Jul. 2019, doi: 10.1109/TPWRS.2019.2894769.

[6] X. Kong, X. Zhang, X. Zhang, C. Wang, H.-D. Chiang, and P. Li, "Adaptive dynamic state estimation of distribution network based on interacting multiple model," *IEEE Trans. Sustain. Energy*, vol. 13, no. 2, pp. 643–652, Apr. 2022, doi: 10.1109/TSTE.2021.3118030.

[7] P. Ju, F. Wu, Q. Chen, J. Han, Y. Tang, and Y. Fan, "Modeling methods for electric loads in a real power grid," in *Proc. 5th Int. Conf. Electr. Electron. Eng. (ICEEE)*, May 2018, pp. 166–172, doi: 10.1109/ICEEE2.2018.8391323.

[8] M. C. Di Piazza, M. Luna, and G. Vitale, "Dynamic PV model parameter identification by least-squares regression," *IEEE J. Photovolt.*, vol. 3, no. 2, pp. 799–806, Apr. 2013, doi: 10.1109/JPHOTOV.2012.2236146.

[9] X. Liang, "Emerging power quality challenges due to integration of renewable energy sources," *IEEE Trans. Ind. Appl.*, vol. 53, no. 2, pp. 855–866, Mar./Apr. 2017, doi: 10.1109/TIA.2016.2626253.

[10] G. Durgaprasad and S. S. Thakur, "Robust dynamic state estimation of power systems based on M-estimation and realistic modeling of system dynamics," *IEEE Trans. Power Syst.*, vol. 13, no. 4, pp. 1331–1336, Nov. 1998.

[11] G. Valverde and V. Terzija, "Unscented Kalman filter for power system dynamic state estimation," *IET Generat., Transmiss. Distrib.*, vol. 5, no. 1, pp. 29–37, Jan. 2011.

[12] A. Sharma, S. C. Srivastava, and S. Chakrabarti, "A cubature Kalman filter based power system dynamic state estimator," *IEEE Trans. Instrum. Meas.*, vol. 66, no. 8, pp. 2036–2045, Aug. 2017.

[13] A. K. Sinha and J. K. Mondal, "Dynamic state estimator using ANN based bus load prediction," *IEEE Trans. Power Syst.*, vol. 14, no. 4, pp. 1219–1225, Nov. 1999.

[14] N. R. Shivakumar and A. Jain, "A review of power system dynamic state estimation techniques," in *Proc. Joint Int. Conf. Power Syst. Technol. IEEE Power India Conf.*, Oct. 2008, pp. 1–6, doi: 10.1109/ICPST.2008.4745312.

[15] M. Huang, Z. Wei, G. Sun, Y. Sun, H. Zang, and K. W. Cheung, "A historical data-driven unscented Kalman filter for distribution system state estimation," in *Proc. IEEE Power Energy Soc. Gen. Meeting*, Jul. 2017, pp. 1–5.

[16] S. M. O. Alhalali and R. A. Elshatshat, "State estimator for electrical distribution systems based on a particle filter," in *Proc. IEEE Power Energy Soc. Gen. Meeting*, Jul. 2015, pp. 1–5.

[17] A. M. Kettner and M. Paolone, "Sequential discrete Kalman filter for real-time state estimation in power distribution systems: Theory and implementation," *IEEE Trans. Instrum. Meas.*, vol. 66, no. 9, pp. 2358–2370, Sep. 2017.

[18] C. Carquex, C. Rosenberg, and K. Bhattacharya, "State estimation in power distribution systems based on ensemble Kalman filtering," *IEEE Trans. Power Syst.*, vol. 33, no. 6, pp. 6600–6610, Nov. 2018.

[19] J. Zhao, M. Netto, and L. Mili, "A robust iterated extended Kalman filter for power system dynamic state estimation," *IEEE Trans. Power Syst.*, vol. 32, no. 4, pp. 3205–3216, Jul. 2017.

[20] J. Zhao and L. Mili, "Robust unscented Kalman filter for power system dynamic state estimation with unknown noise statistics," *IEEE Trans. Smart Grid*, vol. 10, no. 2, pp. 1215–1224, Mar. 2019.

[21] L. Chang, B. Hu, A. Li, and F. Qin, "Transformed unscented Kalman filter," *IEEE Trans. Autom. Control*, vol. 58, no. 1, pp. 252–257, Jan. 2013.

[22] L. Dang, W. Wang, and B. Chen, "Square root unscented Kalman filter with modified measurement for dynamic state estimation of power systems," *IEEE Trans. Instrum. Meas.*, vol. 71, pp. 1–13, 2022, doi: 10.1109/TIM.2022.3157005.

[23] I. Arasaratnam and S. Haykin, "Cubature Kalman filters," *IEEE Trans. Autom. Control*, vol. 54, no. 6, pp. 1254–1269, Jun. 2009.

[24] K. Emami, T. Fernando, H. H. C. Iu, H. Trinh, and K. P. Wong, "Particle filter approach to dynamic state estimation of generators in power systems," *IEEE Trans. Power Syst.*, vol. 30, no. 5, pp. 2665–2675, Sep. 2015, doi: 10.1109/TPWRS.2014.2366196.

[25] Q. Meng, H. Leib, and X. Li, "Cubature ensemble Kalman filter for highly dimensional strongly nonlinear systems," *IEEE Access*, vol. 8, pp. 144892–144907, 2020, doi: 10.1109/ACCESS.2020.3014850.

[26] K. Dehghanpour, Y. Yuan, Z. Wang, and F. Bu, "A game-theoretic data-driven approach for pseudo-measurement generation in distribution system state estimation," *IEEE Trans. Smart Grid*, vol. 10, no. 6, pp. 5942–5951, Nov. 2019.

[27] M. E. Baran, J. Zhu, and A. W. Kelley, "Meter placement for real-time monitoring of distribution feeders," *IEEE Trans. Power Syst.*, vol. 11, no. 1, pp. 332–337, Feb. 1996.

[28] A. Shafiu, N. Jenkins, and G. Strbac, "Measurement location for state estimation of distribution networks with generation," *IEE Proc., Generat., Transmiss. Distrib.*, vol. 152, no. 2, pp. 240–246, Mar. 2005.

[29] A. Primadianto and C.-N. Lu, "A review on distribution system state estimation," *IEEE Trans. Power Syst.*, vol. 32, no. 5, pp. 3875–3883, Sep. 2016.

[30] P. A. Pegoraro, A. Angioni, M. Pau, A. Monti, C. Muscas, F. Ponci, and S. Sulis, "Bayesian approach for distribution system state estimation with non-Gaussian uncertainty models," *IEEE Trans. Instrum. Meas.*, vol. 66, no. 11, pp. 2957–2966, Nov. 2017.

[31] T. Ahmad and N. Senroy, "An information theoretic approach to power-substation level dynamic state estimation with non-Gaussian noise," *IEEE Trans. Power Syst.*, vol. 35, no. 2, pp. 1642–1645, Mar. 2020, doi: 10.1109/TPWRS.2020.2965795.

[32] S. Wang, J. Zhao, Z. Huang, and R. Diao, "Assessing Gaussian assumption of PMU measurement error using field data," *IEEE Trans. Power Del.*, vol. 33, no. 6, pp. 3233–3236, Dec. 2018, doi: 10.1109/TPWRD.2017.2762927.

[33] N. Zhou, Z. Huang, and D. Meng, "Capturing dynamics in the power grid: Formulation of dynamic state estimation through data assimilation," Pacific Northwest Nat. Lab., Richland, WA, USA, Tech. Rep. PNNL-23213, 2014.

[34] J. Zhao and L. Mili, "A framework for robust hybrid state estimation with unknown measurement noise statistics," *IEEE Trans. Ind. Informat.*, vol. 14, no. 5, pp. 1866–1875, May 2018.

[35] A. Mauroy, I. Mezic, and Y. Susuki, *The Koopman Operator in Systems and Control: Concepts, Methodologies, and Applications* (Lecture Notes in Control and Information Sciences). Cham, Switzerland: Springer, 2020. [Online]. Available: https://link.springer.com/book/10.1007/978-3-030-35713-9#bibliographic-information

[36] M. Budišic, R. Mohr, and I. Mezic, "Applied Koopmanism," *Chaos, Interdiscipl. J. Nonlinear Sci.*, vol. 22, no. 4, 2012, Art. no. 047510.

[37] Y. Susuki and I. Mezić, "Nonlinear Koopman modes and power system stability assessment without models," *IEEE Trans. Power Syst.*, vol. 29, no. 2, pp. 899–907, Mar. 2014, doi: 10.1109/TPWRS.2013.2287235.

[38] K. K. Chen, J. H. Tu, and C. W. Rowley, "Variants of dynamic mode decomposition: Boundary condition, Koopman, and Fourier analyses," *J. Nonlinear Sci.*, vol. 22, no. 6, pp. 887–915, Mar. 2012.

[39] Y. Susuki, I. Mezi, and T. Hikihara, "Coherent swing instability of power grids," *J. Nonlinear Sci.* vol. 21, no. 3, pp. 403–439, 2011.

[40] S. Jafarzadeh, I. Genc, and A. Nehorai, "Real-time transient stability prediction and coherency identification in power systems using Koopman mode analysis," *Electr. Power Syst. Res.*, vol. 201, Dec. 2021, Art. no. 107565.

[41] C. Schütte, P. Koltai, and S. Klus, "On the numerical approximation of the Perron–Frobenius and Koopman operator," *J. Comput. Dyn.*, vol. 3, no. 1, pp. 51–79, 2017.

[42] M. Netto, Y. Susuki, and L. Mili, "Data-driven participation factors for nonlinear systems based on Koopman mode decomposition," *IEEE Control Syst. Lett.*, vol. 3, no. 1, pp. 198–203, Jan. 2019, doi: 10.1109/LCSYS.2018.2871887.

[43] A. Surana and A. Banaszuk, "Linear observer synthesis for nonlinear systems using Koopman operator framework," *IFAC-PapersOnline*, vol. 49, no. 18, pp. 716–723, 2016.

[44] M. O. Williams, I. G. Kevrekidis, and C. W. Rowley, "A data–driven approximation of the Koopman operator: Extending dynamic mode decomposition," *J. Nonlinear Sci.*, vol. 25, no. 6, pp. 1307–1346, 2015, doi: 10.1007/s00332-015-9258-5.

[45] J. H. Tu, C. W. Rowley, D. M. Luchtenburg, S. L. Brunton, and J. N. Kutz, "On dynamic mode decomposition: Theory and applications," *J. Comput. Dyn.*, vol. 1, no. 2, pp. 391–421, 2015.

[46] S. L. Brunton, J. L. Proctor, and J. N. Kutz, "Discovering governing equations from data by sparse identification of nonlinear dynamical systems," *Proc. Nat. Acad. Sci. USA*, vol. 113, no. 15, pp. 3932–3937, 2016.

[47] G. Grisetti, C. Stachniss, and W. Burgard, "Improving grid-based SLAM with Rao–Blackwellized particle filters by adaptive proposals and selective resampling," in *Proc. IEEE Int. Conf. Robot. Autom.*, Apr. 2005, pp. 2432–2437, doi: 10.1109/ROBOT.2005.1570477.

[48] E. Kaiser, J. N. Kutz, and S. L. Brunton, "Data-driven discovery of Koopman eigenfunctions for control," *Mach. Learn., Sci. Technol.*, vol. 2, no. 3, Sep. 2021, Art. no. 035023.

[49] P. C. Hansen, "Truncated singular value decomposition solutions to discrete ill-posed problems with ill-determined numerical rank," *SIAM J. Sci. Stat. Comput.*, vol. 11, no. 3, pp. 503–518, May 1990.

[50] H. M. Khodr, F. G. Olsina, P. M. D. O.-D. Jesus, and J. M. Yusta, "Maximum savings approach for location and sizing of capacitors in distribution systems," *Electr. Power Syst. Res.*, vol. 78, no. 7, pp. 1192–1203, Jul. 2008.
[51] R. D. Zimmerman, C. E. Murillo-Sánchez, and R. J. Thomas, "MATPOWER: Steady-state operations, planning, and analysis tools for power systems research and education," *IEEE Trans. Power Syst.*, vol. 26, no. 1, pp. 12–19, Feb. 2011, doi: 10.1109/TPWRS.2010.2051168.
[52] S. Wang, R. Huang, Z. Huang, and R. Fan, "A robust dynamic state estimation approach against model errors caused by load changes," *IEEE Trans. Power Syst.*, vol. 35, no. 6, pp. 4518–4527, Nov. 2020, doi: 10.1109/TPWRS.2020.2994898.
[53] (2016). *Parallel State Estimation*. Accessed: Aug. 15, 2017. [Online]. Available: http://eioc.pnnl.gov/research/hpc_parallel.stm

KAI WANG received the B.E. degree in electrical engineering from Guizhou University, Guiyang, China, in 2018, where he is currently pursuing the master's degree with the Department of Electrical Engineering. His major research interest includes power system state estimation.

MIN LIU received the Ph.D. degree from The University of Hong Kong. She was a Postdoctoral Researcher at The University of Hong Kong, from 2007 to 2008, and a Visiting Scholar at the University of California at Berkeley, Berkeley, CA, USA, from 2013 to 2014. She is currently a Professor and the Vice Dean of the Faculty of Electrical Engineering, Guizhou University, China. Her research interests include smart grid, power system optimization, electricity planning and investment, electricity market, and risk management.

WANG HE was born in Bijie, Guizhou, China, in 1998. He received the B.E. degree in electrical engineering from Guizhou University, China, in 2021, where he is currently pursuing the master's degree in electrical engineering with the School of Electrical Engineering. His research interest includes demand response.

CHAOWEN ZUO was born in Xingyi, Guizhou, China, in 1998. He received the B.E. degree in electrical engineering from Guizhou University, China, in 2021, where he is currently pursuing the master's degree with the Department of Electrical Engineering. His main research interest includes demand response.

FANYUN WANG received the B.E. degree from the School of Energy and Power Engineering, Nanjing Normal University, China, in 2020. She is currently pursuing the master's degree in electrical engineering with the College of Electrical Engineering, Guizhou University. Her current research interest includes demand response.